

# RSC Advances



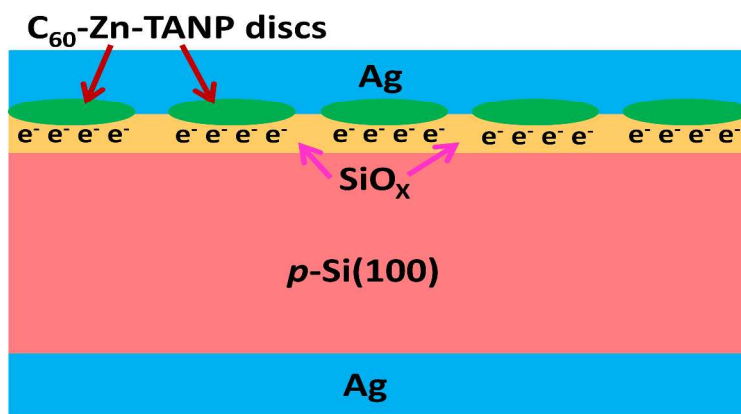
This is an *Accepted Manuscript*, which has been through the Royal Society of Chemistry peer review process and has been accepted for publication.

*Accepted Manuscripts* are published online shortly after acceptance, before technical editing, formatting and proof reading. Using this free service, authors can make their results available to the community, in citable form, before we publish the edited article. This *Accepted Manuscript* will be replaced by the edited, formatted and paginated article as soon as this is available.

You can find more information about *Accepted Manuscripts* in the [Information for Authors](#).

Please note that technical editing may introduce minor changes to the text and/or graphics, which may alter content. The journal's standard [Terms & Conditions](#) and the [Ethical guidelines](#) still apply. In no event shall the Royal Society of Chemistry be held responsible for any errors or omissions in this *Accepted Manuscript* or any consequences arising from the use of any information it contains.

## Graphical Abstract



A MIS-type diode ( $Ag/ C_{60}$ -ZnTANP circular discs / $p$ -Si/Ag) has been fabricated and its charge storage properties have been explored.

Cite this: DOI: 10.1039/coxx00000x

www.rsc.org/xxxxxx

ARTICLE TYPE

## Synthesis, electron transports, and charge storage properties of fullerene–zinc porphyrin hybrid nanodiscs

Antara Garai,<sup>a</sup> Mohit Kumar,<sup>b</sup> Woormileela Sinha,<sup>a</sup> Sriparna Chatterjee<sup>c</sup>, Chandra Shekhar Purohit,<sup>a</sup> Tapobrata Som<sup>\*b</sup> and Sanjib Kar<sup>\*a</sup>

Received (in XXX, XXX) Xth XXXXXXXXX 20XX, Accepted Xth XXXXXXXXX 20XX

DOI: 10.1039/b000000x

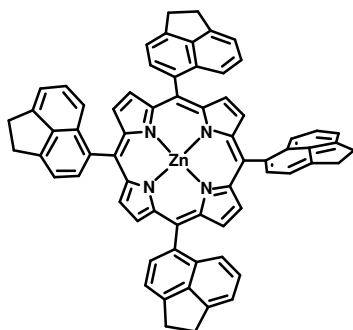
A donor (D)–acceptor (A) based system has been developed with the help of a newly synthesized Zn–porphyrin complex and C<sub>60</sub> fullerene. A series of spectroscopic methods; like absorption spectroscopy (UV–Vis–NIR), Powder X–ray diffraction (XRD), and X–ray photoelectron spectroscopy (XPS) measurements confirm the existence of a charge transfer based complex between Zn–porphyrin and C<sub>60</sub> fullerene. By using this D–A based system, circular discs like nano-objects have been generated. With the help of these nano objects, a diode has been fabricated. The current–voltage (I–V) and the capacitance–voltage (C–V) analysis of the diode are done. The critical role of the Ag–C<sub>60</sub>–Zn–porphyrin and C<sub>60</sub>–Zn–porphyrin–SiO<sub>x</sub> interfaces are clearly understood from the I–V characteristic of the present device. Existence of a hysteresis loop in the C–V plot indicates that the device is indeed suitable for charge storage applications.

### Introduction

Due to its unique physical and chemical properties, fullerenes have found extensive applications in many areas, including *n*-type semiconductors,<sup>1</sup> solar cells,<sup>2</sup> organic field effect transistors,<sup>3</sup> superconductor,<sup>4</sup> and medicine.<sup>5</sup> The major route towards the synthesis of various self-assembled fullerene systems involves chemical modifications of it by attaching various functional groups.<sup>6–10</sup> However, the controlled synthesis of nano- and micro-structures, bearing unmodified fullerene, is still a challenging task. Similarly, porphyrin based materials have also been extensively studied as photoconductors.<sup>11</sup> Uses of porphyrin based nano-architectures as electron transport materials are also explored.<sup>12</sup> Fullerene (C<sub>60</sub>) with triply degenerate lowest unoccupied molecular orbitals (LUMO), which are susceptible to six electrons reduction under ambient conditions and zinc-porphyrin, with large excess of  $\pi$ -electron density and a closed shell central metal like zinc are known to be a potential donor–acceptor pair.<sup>13</sup> These porphyrin–fullerene dyads are known to exhibit rich physical properties,<sup>14</sup> viz. metallic,<sup>15</sup> magnetic,<sup>16</sup> luminescent,<sup>17</sup> and non-linear optical (NLO) properties.<sup>18</sup> Recently, polymer (D)-fullerene (A) pair has been successfully used in organic photovoltaic devices and was observed that the device performance was highly dependent on the morphology of each of the components.<sup>19–21</sup> Thus, it can be assumed that the donor (D)–acceptor (A) based nano-architectures will have tremendous potential for the development of various micro/ nano-

sized devices. In this context, porphyrin–fullerene dyads will be a perfect choice to design various nano-architectures and test their suitability for various practical applications in materials science. Till date, only limited information is available regarding the nano-architectures bearing porphyrin–fullerene dyads.<sup>22–28</sup> Very recently, Wakahara *et al.*<sup>29</sup> synthesized fullerene–cobalt porphyrin hybrid nanosheets which exhibit ambipolar characteristics. Kamat *et al.*<sup>30</sup> have prepared fullerene–porphyrin nanoclusters and explored its efficacy for the generation of photocurrent. Valli *et al.*<sup>25</sup> prepared thin films of porphyrin–fullerene and measured its effectiveness in solar energy harvesting. Nishino *et al.*<sup>31</sup> has demonstrated that a single fullerene–porphyrin pair can act as a molecular rectifier. Few recent reports also demonstrate the usefulness of Langmuir–Blodgett (LB) films composed of fullerene–porphyrin layers as efficient current rectifier.<sup>32–33</sup> To the best of our knowledge, a porphyrin (D)–fullerene (A) based nano-architecture has never been exploited as a metal–insulator–semiconductor (MIS) diode with potential implications in charge storage.<sup>34</sup> A novel zinc-porphyrin complex, [5,10,15,20-tetra(5-acenaphthyl)porphinato] zinc(II), ZnTANP has been synthesized for the first time. The structure of ZnTANP is shown in Scheme 1. ZnTANP, which has a flat concave aromatic surface in the close packed 3-D structure, was used to form supramolecular assemblies with the C<sub>60</sub> molecule. Herein we report the synthesis and characterization of novel C<sub>60</sub>–ZnTANP hybrid materials. Well-defined circular disc-like 3D nanostructures were obtained from C<sub>60</sub>–ZnTANP solutions in benzene under suitable

experimental conditions. By using these  $C_{60}$ -ZnTANP circular discs, a diode was fabricated having the following configuration Ag/ $C_{60}$ -ZnTANP circular discs/*p*-Si/Ag. The current rectification properties of this MIS-type diode and its application as a charge storage device have also been explored in this work.



**Scheme 1** Molecular structures of the ZnTANP

## Results and discussion

### Synthesis and Characterization

The reaction of a chloroform solution of the  $H_2$ TANP with the zinc acetate in methanol resulted in formation of the complex, ZnTANP (see ESI<sup>†</sup>). Purity and identity of the ZnTANP is demonstrated by its satisfactory elemental analyses,  $^1H$  NMR, and by the electrospray mass spectral data (see ESI<sup>†</sup>, Fig.S1 & Fig. S2). ZnTANP exhibited two successive well-resolved reversible oxidative couples at 0.27V and 0.51 V. It also showed one well-defined reductive couple at 1.91 V *versus* ferrocene/ferricinium. The  $C_{60}$ -ZnTANP hybrid material was synthesized by slight modifications of a protocol (see Experimental Section) developed by Wakahara *et al.*<sup>29</sup> Novel  $C_{60}$ -ZnTANP circular discs were synthesized by evaporating a solution of  $C_{60}$ -ZnTANP in benzene solution on the silicon substrates by applying spin coating method. Scanning electron microscopy (SEM) images of  $C_{60}$ -ZnTANP circular disc-like objects are shown in Fig. 1, which shows a uniform distribution. The average size of the discs is ~250 nm in diameter. Energy dispersive x-ray spectroscopic (EDS) analysis was also performed to analyze the composition of the circular discs. This clearly demonstrates the presence of C, N, and Zn in percentages very near to the 1:1 complex between  $C_{60}$  and ZnTANP in the hybrid material (Fig. S3). Thus, it could be tentatively assigned as 1:1 complex formation between  $C_{60}$  and ZnTANP.

### Growth mechanism

In order to get an insight into the growth mechanism, the drying processes of the  $C_{60}$ -ZnTANP hybrid material in benzene solution and also several other key conditions (which affects the drying processes), viz. drying inside the desiccators, drying in open air etc. were carefully monitored. In addition, both drop casting and spin coating methods were also performed. The main purpose of all these experiments was to capture few intermediate structures. Careful observations revealed that in few of these cases  $C_{60}$ -ZnTANP circular discs were obtained with varying sizes. However, in few of the selected sets we were able to

capture a series of intermediate sized nanoparticles. It was also observed that when the drying process was very fast, a sizeable number of nanoparticles, having disc-like shapes, were also obtained with their average diameter much lesser than the final nano-discs. In addition, a series of fused dimers and trimers of nano-discs were also obtained. Based on all these intermediate structures, a tentative mechanism has been proposed towards the formation of  $C_{60}$ -ZnTANP circular nano-discs. It is assumed that during the evaporation process of the  $C_{60}$ -ZnTANP hybrid materials in benzene, initially smaller sized nanoparticles are formed. Then these smaller particles assemble and form smaller sized discs. Finally these smaller sized nano-discs aggregate further and form bigger sized nano-discs as shown in Fig. 2.

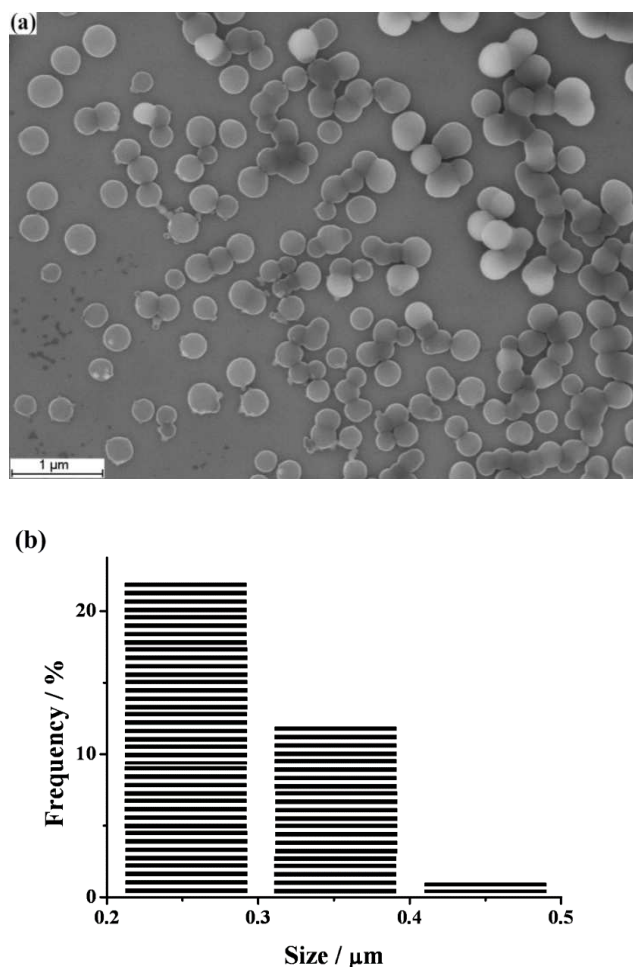


**Fig. 1** (a) Scanning electron microscopy (SEM) images of the  $C_{60}$ -ZnTANP circular disc, after evaporation of the benzene solution on the Si substrates and (b) size distribution histograms of circular discs.

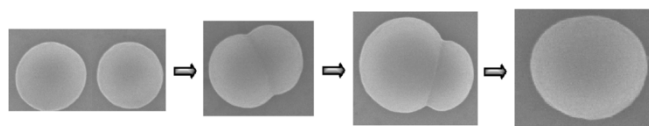


**Fig. 2** Plausible mechanism of  $C_{60}$ -ZnTANP circular nano-disc formation via aggregations of smaller sized nano-discs.

### X-ray structural studies of ZnTANP

The crystal structure analysis of ZnTANP was performed to analyze its tendency to form supramolecular assemblies. The crystal structure of ZnTANP is shown in Fig. 3. Important crystallographic parameters are presented in Table 1. From the crystal structure analysis of ZnTANP, it is observed that the molecules are stacked together by various weak Van der Waals forces-like  $\pi$ - $\pi$  stacking interaction ( $\sim 0.364$  nm), C-H...N interactions ( $\sim 0.267$  nm) and form closely-packed 3D structures in the packing diagram (Fig. 4).<sup>35</sup>

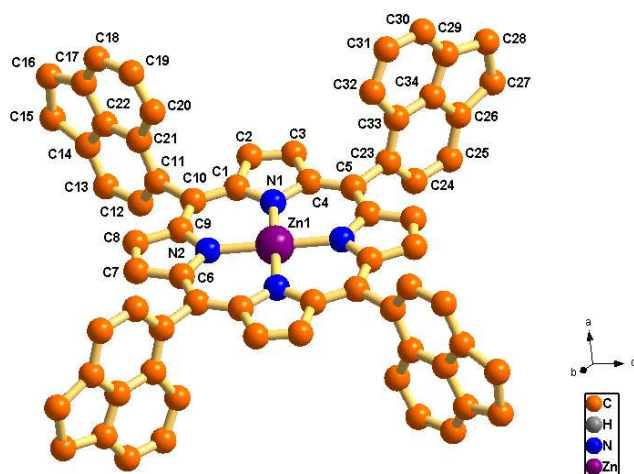


**Fig. 3** Single-crystal X-ray structure of ZnTANP.

Along the crystallographic  $c$ -axis it appears that these 3D structures have flat aromatic surfaces. It is assumed that these flat aromatic surfaces facilitate the formation of supramolecular assemblies with the  $C_{60}$  molecules.

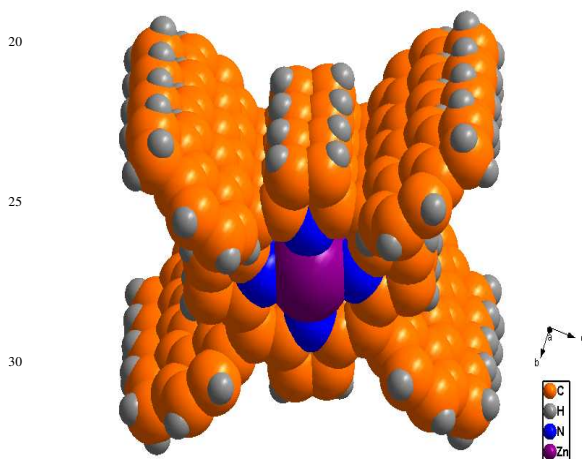


**Fig. 4** Orientation of zinc atoms in single-crystal X-ray structure of ZnTANP when viewed along  $c$ -axis.

**Table 1** Crystallographic data for ZnTANP

molecular formula	$C_{34}H_{22}N_2Zn_{0.5}$
Fw	491.22
Radiation	MoK $\alpha$
crystal symmetry	Triclinic
space group	P -1
$a$ ( $\text{\AA}$ )	8.393(5)
$b$ ( $\text{\AA}$ )	11.628(5)
$c$ ( $\text{\AA}$ )	14.178(5)
$a$ (deg)	90.808(5)
$\beta$ (deg)	91.990(5)
$\gamma$ (deg)	93.628(5)
$V$ ( $\text{\AA}^3$ )	1379.9(11)
Z	2
$\mu$ ( $\text{mm}^{-1}$ )	0.489
$T$ (K)	293(2) K
$D_{\text{calcd}}$ ( $\text{g cm}^{-3}$ )	1.182
$2\theta$ range (deg)	4.86 to 48.38
$e$ data ( $R_{\text{int}}$ )	4305 (0.0364)
R1 ( $I > 2\sigma(I)$ )	0.0967
WR2	0.2467
GOF	1.098

### Electronic spectra

In order to confirm the charge-transfer (CT) complex formation, the UV-vis-NIR spectroscopy was used to monitor the charge-transfer transitions between ZnTANP and  $C_{60}$ . Moderately weak absorption band in the visible region with maxima at around 860 nm in the  $C_{60}$ -ZnTANP hybrid material was observed (Fig. 5).

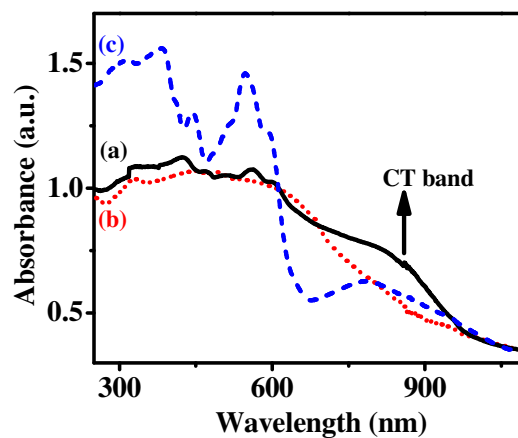


**Fig. 5** UV-vis-NIR spectra of the (a)  $C_{60}$ -ZnTANP hybrid material (—), (b)  $C_{60}$  powder (.....), and (c) ZnTANP powder (---).

This moderately weak band has been ascribed as charge transfer (CT) band from ZnTANP  $\rightarrow$  C<sub>60</sub> and is well supported by previous reports.<sup>36-37</sup> The CT transition energy corresponding to the absorption band at around 860 nm is equivalent to 1.44 eV.

### 5 X-Ray photoelectron spectroscopy (XPS)

XPS has been used to estimate the change in the distribution of electron density of hetero-atoms of the donors (ZnTANP) upon formation of hybrid material (C<sub>60</sub>-ZnTANP). As all the four nitrogen atoms of ZnTANP are chemically equivalent, they give rise to a single peak in the N 1s region of the XPS spectrum (Fig. 6) and the binding energy of N atoms is 398.43 eV. Similarly there is only one Zn atom in the ZnTANP, which exhibits only one signal at the Zn 2P<sub>3/2</sub> region of the XP spectrum (Fig. 7). The binding energy of the coordinated Zn atom is 1021.32 eV. However in the XP spectrum of C<sub>60</sub>-ZnTANP hybrid material a positive shift is observed for both N 1s (1.7 eV) and Zn 2P<sub>3/2</sub> (0.3 eV) peaks and it clearly indicates the formation of a charge transfer based complex (Fig.s 6 & 7).<sup>38</sup>

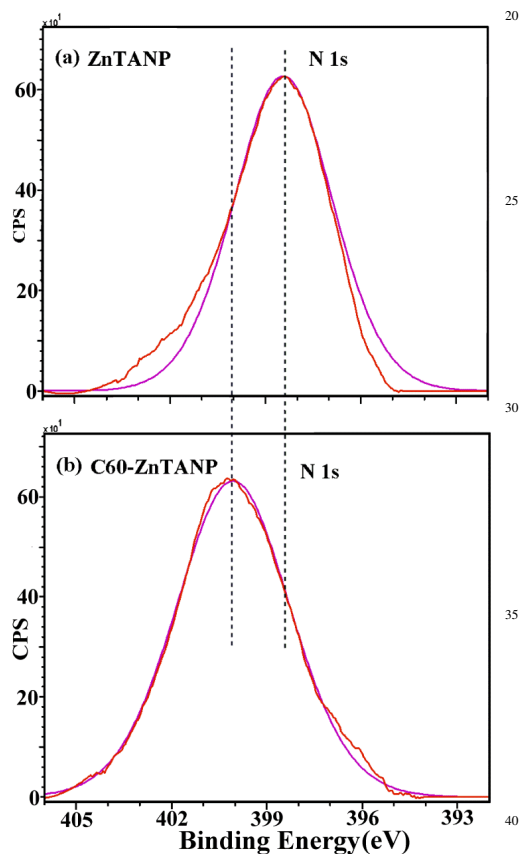


**Fig. 6** N1s region of the X-ray photo electron spectrum of (a) ZnTANP powder, and (b) C<sub>60</sub>-ZnTANP hybrid materials.

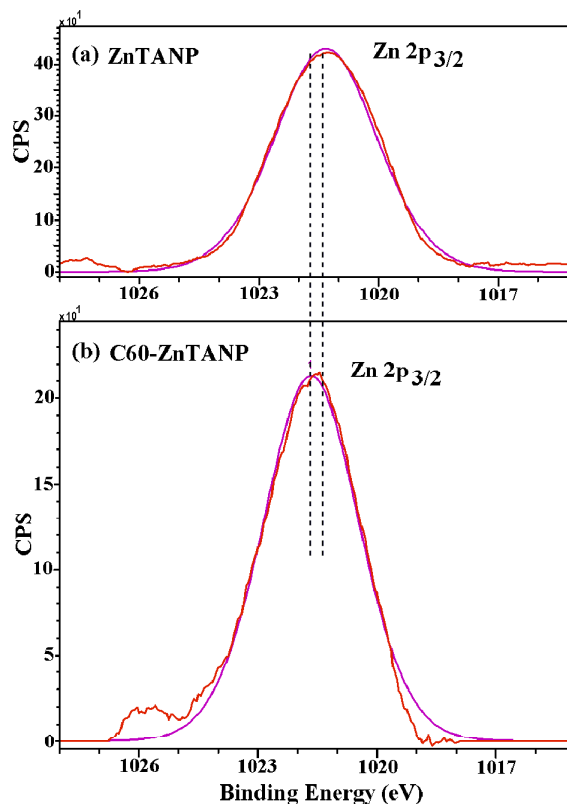


**Fig. 7** Zn2p<sub>3/2</sub> region of the X-ray photo electron spectrum of (a) ZnTANP powder, and (b) C<sub>60</sub>-ZnTANP hybrid materials.

### X-ray Diffraction (XRD)

The C<sub>60</sub>-ZnTANP circular discs were characterized by X-ray diffraction (XRD) measurements. XRD patterns of the ZnTANP, C<sub>60</sub>-fullerene and C<sub>60</sub>-ZnTANP circular discs are shown in Fig. 8. The XRD pattern of the C<sub>60</sub>-ZnTANP circular discs is entirely different from both the starting materials ZnTANP and C<sub>60</sub>-fullerene. For C<sub>60</sub>-fullerene, characteristic eight peaks are observed<sup>39</sup> and indexed as (111), (220), (311), (222), (331), (420), (422), and (511) / (333) and are typical of its fcc structure. C<sub>60</sub>-ZnTANP circular discs exhibit few broad and few sharp and intense peaks. It appears that overlapping of C<sub>60</sub>-fullerene and ZnTANP signals occurs and results in the broadening of the spectrum. However, the characteristic peaks of both C<sub>60</sub>-fullerene and ZnTANP are present on the C<sub>60</sub>-ZnTANP circular discs.

### 65 I-V characteristics

In order to analyze the current-voltage (I-V) characteristics, two types of diodes have been fabricated with the following configurations (see the Experimental methods): (1) Ag/C<sub>60</sub>-ZnTANP circular discs/p-Si/Ag and (2) pristine Si based heterojunction diode (Ag/p-Si/Ag). A non-ideal rectifying current-voltage characteristics has been observed in both the cases (Fig. 9).<sup>40</sup> The turn-on potential ( $V_T$ ) and reverse break down voltage increases from 2.15 V to 3.15 V and 2.08 V to 8.17 V, respectively, for C<sub>60</sub>-ZnTANP based diode in comparison to pristine silicon based diode. The rectification ratio ( $r$ ) of a diode is expressed by  $r = I_f / I_r$ , where  $I_f$  is the forward current, and  $I_r$  is

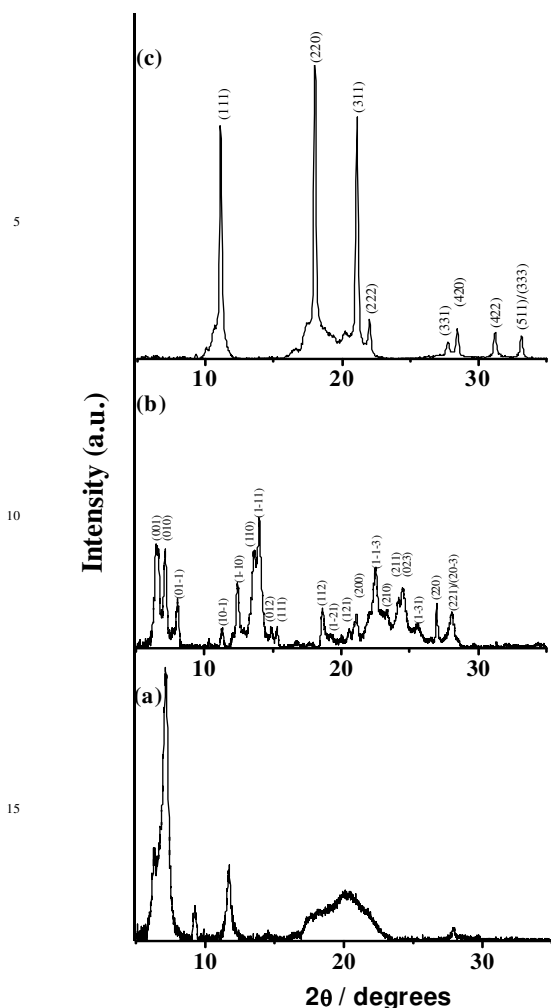


**Fig. 8** XRD patterns of the (a)  $C_{60}$ -ZnTANP circular discs, (b) ZnTANP powder, and (c)  $C_{60}$  powder.

the reverse current.<sup>40</sup> By using this equation, a rectification factor of 100 is obtained at 3 V. The composition of the first diode (*vide supra*), clearly points towards a MIS (metal, insulator layer, and semiconductor) diode.<sup>40</sup> By adding an insulating layer (native oxide layer on a Si substrate), the characteristics of the diode was found to change drastically. Upon applying a bias voltage, the interfacial state (it exists between the junction of  $SiO_x$  {native oxide layer} and  $C_{60}$ -ZnTANP circular discs) is getting charged and an additional field is generated.<sup>40</sup> Thermionic emission theory has been frequently used to explain the characteristics of the MIS diode.<sup>40</sup> The characteristics of such a diode can be easily approximated by the following  $I$ - $V$  equation as:  $I = I_0 \exp(qV/nk_B T)$  when  $V > 3k_B T/q$ , where  $q$  is the unit charge,  $V$  is the voltage (applied),  $k_B$  is Boltzmann constant,  $n$  is the ideality factor, and  $T$  is the temperature.<sup>40,41</sup> The following equation  $\{n = [q/k_B T] \cdot [dV/d(\ln I)]\}$  has been frequently used to calculate the ideality factor ( $n$ ) of the diode.<sup>40,41</sup> The ideality factor ( $n$ ) of the present diode has been found to be  $\sim 1.46$ . The  $n$  value indicates that the present diode is not an ideal Schottky barrier diode; instead it is a MIS-type diode.<sup>40</sup> As both

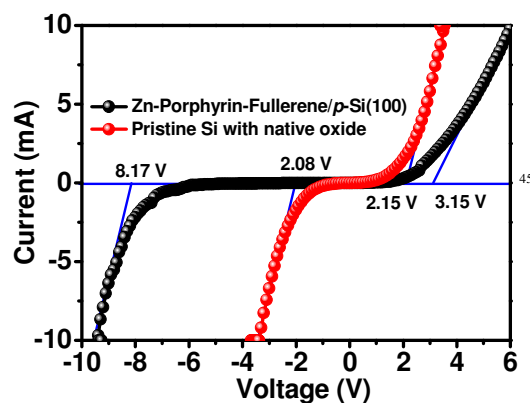


**Fig. 9** Nonlinear  $I$ - $V$  characteristics of  $Ag/C_{60}$ -ZnTANP circular discs /  $p$ -Si/Ag diodes. The black solid line represents the  $I$ - $V$  characteristics of  $Ag/C_{60}$ -ZnTANP circular discs /  $p$ -Si/Ag diodes and the red line are for the  $Ag/p$ -Si/Ag diodes (colour online).

the charge trapping and charge recombination processes are absent in the ideal situation,<sup>42</sup> the ideality factor of the diode is thus equals to unity. The  $I$ - $V$  curve of the present diode has two parts: (a) a linear region, and (b) an exponential region. The linear behaviour is predominantly observed up to the voltage of 1.4 V and the exponential behaviour is observed in the following region;  $1.4 < V_f < 3.15$  V. The exponential behaviour, which is observed at the higher forward bias voltages ( $1.4 < V_f < 3.15$  V), is fully dictated by the diode characteristics, however the linear behaviour, which is observed at the lower voltage sides ( $V_0 = 1.4$  V), is certainly not controlled by the diode characteristics fully and is dependent on certain other factors.<sup>43</sup> Information regarding the recombination processes and the shape of the interfaces (i.e. internal bulk morphology) are obtained from the ideality factor ( $n$ ). Ideality factor ( $n$ ), and the reverse saturation current ( $I_0$ ) controls the  $I$ - $V$  characteristics of a device in the exponential region.<sup>41</sup> In fact, the  $Ag/C_{60}$ -ZnTANP/ $SiO_x/p$ -Si/Ag structure has four interfaces: (i)  $Ag - C_{60}$ -ZnTANP, (ii)  $C_{60}$ -ZnTANP -  $SiO_x$ , (iii)  $SiO_x - p$ -Si, and (iv)  $p$ -Si -  $Ag$ . The electrical properties of heterostructure ( $Ag/C_{60}$ -ZnTANP/ $SiO_x/p$ -Si/Ag) diodes are solely dependent on the interface. Thus it is highly possible that the presence of  $SiO_x - p$ -Si and  $p$ -Si -  $Ag$  interfaces can also influence the diode characteristics. To rule out that possibility, we have constructed a device;  $Ag/SiO_x/p$ -Si/Ag, and checked its  $I$ - $V$  characteristics. The obtained symmetric  $I$ - $V$  characteristic clearly ruled out the involvement of  $SiO_x - p$ -Si and  $p$ -Si -  $Ag$  interfaces. This clearly indicates that the electrical characteristic of the  $Ag/C_{60}$ -ZnTANP/ $SiO_x/p$ -Si/Ag diode is largely controlled by  $Ag - C_{60}$ -ZnTANP and  $C_{60}$ -ZnTANP -  $SiO_x$  interfaces. Thus the depletion region in the  $C_{60}$ -ZnTANP circular discs/ $SiO_x/Si$  interface controls the exponential region of the  $I$ - $V$  characteristics in the device. To garner further support and to understand the current conduction pathways in the device, cAFM measurements were carried out. Stable images were obtained after scanning the different regions of the device with repeating cycles and it was confirmed that the  $C_{60}$ -ZnTANP circular discs are bound

strongly at the device surface. cAFM current maps at 10 V bias show bright spots with  $\sim 100$  pA intensity (Fig. 10). These observed bright spots (Fig. 10) are assigned as leakage current and are responsible for the conduction properties in the device.

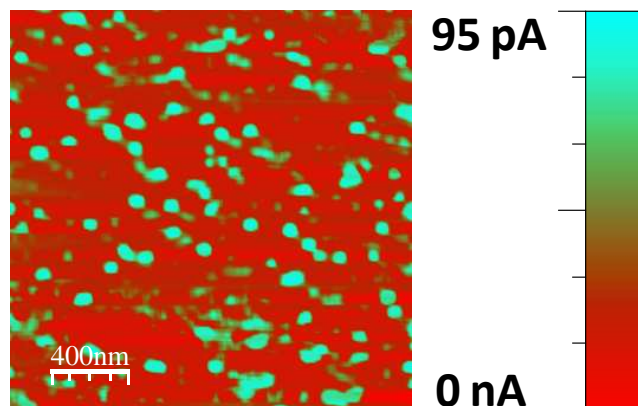


**Fig. 10** CAFM micrographs ( $2\mu\text{m}\times 2\mu\text{m}$ ) of  $\text{C}_{60}$ -ZnTANP circular discs deposited on Si (colour online).

#### C-V characteristics

The critical role of the interface is clearly understood from the  $I$ - $V$  characteristic of the present device and this phenomenon has tempted us to measure the charge storage capability of our device. The corresponding  $C$ - $V$  curves have been obtained by sweeping a voltage from inversion to accumulation regions of the  $\text{C}_{60}$ -ZnTANP circular disc containing layer on Si surface (Fig. 11) at R. T.

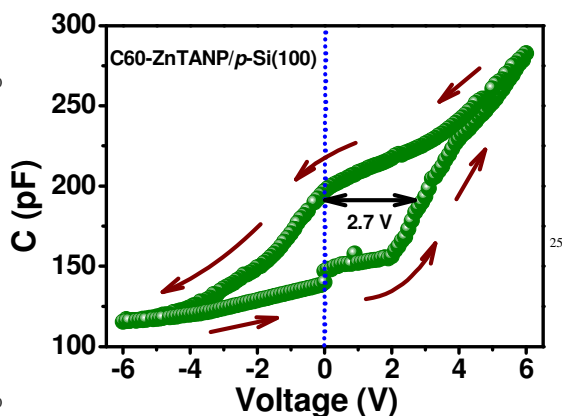


**Fig. 11** A voltage dependent capacitance of  $\text{Ag}/\text{C}_{60}$ -ZnTANP circular discs/ $p$ -Si/ $\text{Ag}$  hetero structure diode (colour online).

In general, hysteresis behaviour in the Capacitance-Voltage plot gives a first hand idea about the suitability of a device in charge storage applications.<sup>44</sup> Thus, here, the observed counter-clockwise hysteresis is a clear signature of the charge-trapping phenomena and a positive shift in voltage ( $\sim 2.7$  V) indicates that those trapped charges are electrons only.<sup>44</sup> It's worth mentioning here that in the  $\text{Ag}/\text{SiO}_2/\text{Si}$  junction, there no such hysteresis

window is observed and it clearly indicates that charge trapping phenomena is nowhere involved in the  $\text{SiO}_2$  and Si interface. Carrier injection model has been successfully employed to explain this kind of hysteresis curve and it is further inferred that the polarity of the bias voltage is fully responsible for the injection of electrons and holes.<sup>44</sup> Thus it can be concluded that the trapped electrons residing in the sandwiched  $\text{C}_{60}$ -ZnTANP circular discs/ $\text{SiO}_x$  are responsible for this hysteresis phenomena. It is obvious that because of the very low thickness ( $\sim 2$  nm) of the native oxide layer, the other alternatives, like  $\text{SiO}_x/\text{Si}$  interface, or the oxide layers are clearly ruled out from the perspectives of charge storage capabilities. Thus it is evident that the trapped charges can reside only at the  $\text{C}_{60}$ -ZnTANP circular discs/ $\text{SiO}_x$  interface. A schematic description of the device is shown in Fig. 12.

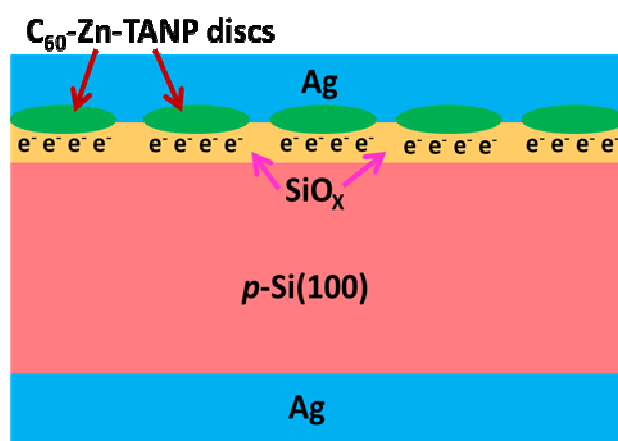


**Fig. 12** Charge transport across the potential barriers is shown schematically for the hetero-structure diode  $\text{Ag}/\text{C}_{60}$ -ZnTANP circular discs/ $p$ -Si/ $\text{Ag}$  (colour online).

Thus in the forward cycle electrons are trapped at the interface and in the reverse cycle they are neutralized by holes. These trapped electrons at the interface generate an additional electric field and thus helps to reduce the barrier height from 2.7 to 0.97 eV. As a result of this, the lowering of turn-on potential occurred. Thus the occurrence of hysteresis could be attributed due to the influence of  $\text{C}_{60}$ -ZnTANP circular discs/ $\text{SiO}_x$  interfacial state. It has been assumed that the charge transfer across the circular discs occurred via tunneling mechanisms. The amount of charge density trapped in the  $\text{C}_{60}$ -ZnTANP circular discs/ $\text{SiO}_x$  interface can be easily estimated with the help of following equation:  $N_t = \epsilon_0 K \Delta V_{\text{FB}} / et$  where,  $\epsilon_0$  is the permittivity of free space,  $K$  is the dielectric constant of  $\text{C}_{60}$  ( $\sim 4.5$ ),  $\Delta V_{\text{FB}}$  is the shifting of flat-band voltage,  $e$  is the electronic charge, and  $t$  is the thickness of silica layer.<sup>44</sup> The rough amount of charge density stored in the  $\text{C}_{60}$ -ZnTANP circular discs/ $\text{SiO}_x$  interface is estimated to be  $2.24 \times 10^{12} \text{ cm}^{-2}$ .

## Conclusions

In conclusion, a donor (D)–acceptor (A) based hybrid material having 1:1 composition of C<sub>60</sub>–ZnTANP was synthesized by using a simple protocol. Circular disc-like 3D objects with an average size distribution of 250 nm were generated by using drop-casting method. By using these circular disc-like nano-architectures, a MIS-type diode was fabricated with the following composition: Ag/C<sub>60</sub>–ZnTANP circular discs/*p*-Si/Ag. The *I*-*V* characteristic of the device was measured and it shows a non ideal rectifying behavior. *C*-*V* measurements were also performed to analyze the charge storage properties of these circular discs. The observed counter-clock wise hysteresis in the *C*-*V* measurement is a clear signature of the charge-trapping phenomena and a positive shift in voltage (~2.7 V) indicates that those trapped charges are electrons only. The rough amount of charge density stored in the C<sub>60</sub>–ZnTANP circular discs/SiO<sub>x</sub> interface is estimated to be 2.24×10<sup>12</sup> cm<sup>-2</sup>. CAFM current maps at 10 V bias show bright spots with ~100 pA intensity. These bright spots are attributed as leakage current and are responsible for the conduction properties in the device. However, as the *p*-Si substrate is not fully covered by the nanodiscs, thus the possibility of other conduction pathways (Ag/*p*-Si/Ag) in the device also cannot be ruled out completely (*vide supra*). Thus our results reveal that the circular disc-like nano-architectures made from C<sub>60</sub>–ZnTANP hybrid materials strongly influence the diode characteristics but its true nature cannot be ascertained accurately.

## Experimental section

### Materials

The precursors pyrrole, benzonitrile, DDQ (2,3-Dichloro-5,6-dicyano-1,4-benzoquinone), 5-acenaphthene carboxaldehyde, C<sub>60</sub>, Toluene and TEAP (Tetraethyl ammonium perchlorate) were purchased from Aldrich, USA. Zn(OAc)<sub>2</sub>·2H<sub>2</sub>O and Isopropyl alcohol were purchased from Merck, India. Other chemicals were of reagent grade. Hexane and CH<sub>2</sub>Cl<sub>2</sub> were distilled from KOH and CaH<sub>2</sub>, respectively. For spectroscopy and electrochemical studies HPLC grade solvents were used. 5,10,15,20-tetra(5-acenaphthyl) porphyrin, H<sub>2</sub>TANP was prepared by slight modification of an earlier reported synthetic protocol (see ESI<sup>†</sup>).<sup>45</sup>

### Characterization

UV–Vis spectral studies were performed on a Perkin–Elmer LAMBDA-750 spectrophotometer. Emission spectral studies were performed on a Perkin Elmer, LS 55 spectrophotometer using optical cell of 1 cm path length. The fluorescence quantum yields were determined using tetraphenylporphyrin, [TPP] as a reference. Time resolved fluorescence measurements were carried out using a time-correlated single photon counting (TCSPC) spectrometer (Edinburgh, OB 920). The elemental analyses were carried out with a Perkin–Elmer 240C elemental analyzer. The NMR measurements were carried out using a Bruker AVANCE 400 NMR spectrometer. Chemical shifts are expressed in parts per million (ppm) relative to residual chloroform ( $\delta = 7.26$ ). Fourier transformed infrared (FTIR) spectra were recorded on a Perkin–Elmer spectrophotometer with samples prepared as KBr

pellets. Electro spray mass spectra were recorded on a Bruker Micro TOF–QII mass spectrometer. Cyclic voltammetry measurements were carried out using a CH Instruments model CHI1120A electrochemistry system. A glassy–carbon working electrode, a platinum wire as an auxiliary electrode and a saturated calomel reference electrode (SCE) were used in a three–electrode configuration. Tetraethyl ammonium perchlorate (TEAP) was the supporting electrolyte (0.1M) and the concentration of the solution was 10<sup>-3</sup>M with respect to the complex. The oxidation and reduction processes at the positive and negative side of the SCE reference electrode were measured by using a glassy–carbon working electrode. The half wave potential  $E_{298}^0$  was set equal to 0.5( $E_{pa} + E_{pc}$ ), where  $E_{pa}$  and  $E_{pc}$  are anodic and cathodic cyclic voltammetric peak potentials, respectively. The scan rate used was 100 mV s<sup>-1</sup>. For the fabrication of Ag/C<sub>60</sub>–ZnTANP circular discs/*p*-Si/Ag diode, *p*-type Si was used as a substrates. The substrates were cleaned sequentially by de-ionized water, methanol, and finally with acetone by using an ultrasonic bath with average immersion time of 10–15 min. For electrical measurements, *p*-Si (100) (thickness = 500μm) with native oxide (SiO<sub>x</sub>) layer of about 2 nm thickness were used as a substrate and as a bottom electrode. On this SiO<sub>x</sub>, desired order of C<sub>60</sub>–ZnTANP was drop-casted and a silver paste was used to make electrical contacts on the top of C<sub>60</sub>–ZnTANP films and on the back side of the Si substrates. In this way a hybrid structure was fabricated. The formation of Ag/C<sub>60</sub>–ZnTANP/Si/Ag hetero-structure diodes was verified by measuring *I*-*V* characteristics with a source meter (Keithley, 2410). The charge storage properties of this hetero-structure diode were investigated by performing capacitance-voltage (*C*-*V*) measurements at a frequency of 1 MHz by using HP 4284A precision LCR meter. All the measurements were carried out on several sets of samples to ensure the repeatability and reproducibility of the data. Conducting atomic force microscopy (CAFM) was used to measure the local electrical property of the samples. CAFM was carried out by *ex-situ* AFM (Asylum Research, MFP3D) in the contact mode with a Pt coated Si cantilever (from NT-MDT) having a radius of curvature of ~35 nm. For each sample, several images were taken from different regions to check the uniformity and to estimate the average conduction areas. Powder X-ray Diffraction (XRD) patterns of the samples were recorded on a Bruker DAVINCI D8 ADVANCE diffractometer equipped with Cu- K $\alpha$  radiation source with  $\lambda = 0.15406$  nm. XPS measurements of the sample were performed by using a monochromatic Mg K $\alpha$  X-ray source (XPS VG Microtech). SEM images of the nanoparticles were captured by using a field emission gun scanning electron microscope (FEGSEM) system (Zeiss, Germany make, Supra 55).

### Crystal Structure Determination

Single crystals of ZnTANP were grown by slow diffusion of a solution of the metal complexes in diethyl ether into dichloromethane, followed by slow evaporation under atmospheric conditions. The crystal data of ZnTANP were collected on a Bruker Kappa APEX II CCD diffractometer at 293

K. Selected data collection parameters and other crystallographic results are summarized in Table 1. All data were corrected for Lorentz polarization and absorption effects. The program package SHELXTL<sup>46</sup> was used for structure solution and full matrix least squares refinement on F<sup>2</sup>. Hydrogen atoms were included in the refinement using the riding model. Contributions of H atoms for the water molecules were included but were not fixed. Disordered solvent molecules were taken out using SQUEEZE<sup>47</sup> command in PLATON. CCDC 982272 contains the supplementary crystallographic data's for ZnTANP. These data can be obtained free of charge via [www.ccdc.cam.ac.uk/data\\_request/cif](http://www.ccdc.cam.ac.uk/data_request/cif).

### Preparation of C<sub>60</sub>-ZnTANP hybrid material

The C<sub>60</sub>-ZnTANP hybrid material was synthesized by following a standard protocol developed by Wakahara *et al.*<sup>29</sup> In a standard protocol, a 10 ml C<sub>60</sub> saturated toluene solution was prepared as a stock solution in a 10 ml volumetric flask. Aliquot of 4 ml was taken from this solution and was mixed with 8.5 mg of ZnTANP in a glass bottle. The solution mixture was then stirred well at room temperature by using ultrasonication. The resulting mixture was kept at a refrigerator (4°C) for 1 h. 8 ml of isopropyl alcohol was added slowly to this mixture; the combined solution was shaken vigorously and was kept in fridge again for overnight. The resulted precipitate was collected, washed thoroughly with toluene, and dried in a vacuum.

### Acknowledgements

Financial support received from the Department of Atomic Energy, Government of India is gratefully acknowledged. Authors thankfully acknowledge NISER, Bhubaneswar and IOP, Bhubaneswar for providing infrastructure and instrumental supports.

### Notes and references

<sup>a</sup>School of Chemical Sciences, National Institute of Science Education and Research (NISER), Bhubaneswar – 751005, India. E-mail: [sanjib@niser.ac.in](mailto:sanjib@niser.ac.in)

<sup>b</sup>Institute of Physics, Sachivalaya Marg, Bhubaneswar – 751005, India. E-mail: [tsom@iopb.res.in](mailto:tsom@iopb.res.in)

<sup>c</sup>Colloids and Material Chemistry Department, Institute of Minerals and Materials Technology (CSIR), Bhubaneswar-751013, India.

† Electronic Supplementary Information (ESI) available: Synthesis and characterization of H<sub>2</sub>TANP and ZnTANP. <sup>1</sup>H NMR and ESI-MS spectrum of ZnTANP. EDS spectrum of the C<sub>60</sub>-ZnTANP circular discs. CCDC 982272 contains the supplementary crystallographic data for ZnTANP. These data can be obtained free of charge via [www.ccdc.cam.ac.uk/data\\_request/cif](http://www.ccdc.cam.ac.uk/data_request/cif).

- H. Yamaoka, *JETI*, 2011, **59**, 37-42.
- N. Camaioni, L. Garlaschelli, A. Geri, M. Maggini, G. Possamai and G. Ridolfi, *J. Mater. Chem.*, 2002, **12**, 2065-2070.
- M. Irimia-Vladu, N. Marjanovic, A. Vlad, A. M. Ramil, G. Hernandez-Sosa, R. Schwoediauer, S. Bauer and N. S. Sariciftci, *Adv. Mater. (Weinheim, Ger.)*, 2008, **20**, 3887-3892.
- M. Ricco, M. Bisbiglia, R. D. Renzi and F. Bolzoni, *Solid State Commun.*, 1997, **101**, 413-416.
- S. Bosi, R. T. Da, G. Spalluto and M. Prato, *Eur. J. Med. Chem.*, 2003, **38**, 913-923.

- T. Nakanishi, W. Schmitt, T. Michinobu, D. G. Kurth and K. Ariga, *Chem. Commun. (Cambridge, U. K.)*, 2005, 5982-5984.
- T. Nakanishi, K. Ariga, T. Michinobu, K. Yoshida, H. Takahashi, T. Teranishi, H. Mohwald and D. G. Kurth, *Small*, 2007, **3**, 2019-2023.
- T. Nakanishi, T. Michinobu, K. Yoshida, N. Shirahata, K. Ariga, H. Mohwald and D. G. Kurth, *Adv. Mater. (Weinheim, Ger.)*, 2008, **20**, 443-446.
- J. Wang, Y. Shen, S. Kessel, P. Fernandes, K. Yoshida, S. Yagai, D. G. Kurth, H. Mohwald and T. Nakanishi, *Angew. Chem., Int. Ed.*, 2009, **48**, 2166-2170.
- T. Nakanishi, N. Miyashita, T. Michinobu, Y. Wakayama, T. Tsuruoka, K. Ariga and D. G. Kurth, *J. Am. Chem. Soc.*, 2006, **128**, 6328-6329.
- T. Shimidzu, H. Segawa, F. Wu and N. Nakayama, *J. Photochem. Photobiol., A*, 1995, **92**, 121-127.
- A. D. Schwab, D. E. Smith, B. Bond-Watts, D. E. Johnston, J. Hone, A. T. Johnson, P. J. C. De and W. F. Smith, *Nano Lett.*, 2004, **4**, 1261-1265.
- J.-B. Giguere and J.-F. Morin, *Org. Biomol. Chem.*, 2012, **10**, 1047-1051.
- D. V. Konarev and R. N. Lyubovskaya, *Russ. Chem. Rev.*, 1999, **68**, 19-38.
- H. Moriyama, H. Kobayashi, A. Kobayashi and T. Watanabe, *Chem. Phys. Lett.*, 1995, **238**, 116-121.
- P. W. Stephens, D. Cox, J. W. Lauher, L. Mihaly, J. B. Wiley, P. M. Allemand, A. Hirsch, K. Holczer, Q. Li and a. et, *Nature (London)*, 1992, **355**, 331-332.
- V. V. Kveder, E. A. Steinman, B. Z. Narymbetov, S. S. Khasanov, L. P. Rozenberg, R. P. Shibaeva, A. V. Bazhenov, A. V. Gorbunov, M. Y. Maksimuk, D. V. Konarev, R. N. Lyubovskaya and Y. A. Ossipyan, *Chem. Phys.*, 1997, **216**, 407-415.
- F. Kajzar, Y. Okada-Shudo, C. Meritt and Z. Kafafi, *Synth. Met.*, 1998, **94**, 91-98.
- M. Campoy-Quiles, T. Ferenczi, T. Agostinelli, P. G. Etchegoin, Y. Kim, T. D. Anthopoulos, P. N. Stavrinou, D. D. C. Bradley and J. Nelson, *Nat. Mater.*, 2008, **7**, 158-164.
- H. Hoppe and N. S. Sariciftci, *J. Mater. Chem.*, 2006, **16**, 45-61.
- J. Peet, M. L. Senatore, A. J. Heeger and G. C. Bazan, *Adv. Mater. (Weinheim, Ger.)*, 2009, **21**, 1521-1527.
- X. Zhang and M. Takeuchi, *Angew Chem Int Ed Engl*, 2009, **48**, 9646-9651.
- P. D. W. Boyd and C. A. Reed, *Acc. Chem. Res.*, 2005, **38**, 235-242.
- K. Tashiro and T. Aida, *Chem. Soc. Rev.*, 2007, **36**, 189-197.
- V. Sgobba, G. Giancane, S. Conoci, S. Casilli, G. Ricciardi, D. M. Guldi, M. Prato and L. Valli, *J. Am. Chem. Soc.*, 2007, **129**, 3148-3156.
- V. Georgakilas, F. Pellarini, M. Prato, D. M. Guldi, M. Melle-Franco and F. Zerbetto, *Proc. Natl. Acad. Sci. U. S. A.*, 2002, **99**, 5075-5080.
- T. Yamaguchi, N. Ishii, K. Tashiro and T. Aida, *J. Am. Chem. Soc.*, 2003, **125**, 13934-13935.
- S. Yoshimoto, E. Tsutsumi, Y. Honda, Y. Murata, M. Murata, K. Komatsu, O. Ito and K. Itaya, *Angew. Chem., Int. Ed.*, 2004, **43**, 3044-3047.
- T. Wakahara, P. D'Angelo, K. i. Miyazawa, Y. Nemoto, O. Ito, N. Tanigaki, D. D. C. Bradley and T. D. Anthopoulos, *J. Am. Chem. Soc.*, 2012, **134**, 7204-7206.
- T. Hasobe, H. Imahori, S. Fukuzumi and P. V. Kamat, *J. Phys. Chem. B*, 2003, **107**, 12105-12112.
- T. Nishino, T. Ito and Y. Umezawa, *Proc. Natl. Acad. Sci. U. S. A.*, 2005, **102**, 5659-5662.

- 32 R. M. Metzger, J. W. Baldwin, W. J. Shumate, I. R. Peterson, P. Mani, G. J. Mankey, T. Morris, G. Szulczewski, S. Bosi, M. Prato, A. Comito and Y. Rubin, *J. Phys. Chem. B*, 2003, **107**, 1021-1027.
- 33 S. P. Koiry, P. Jha, D. K. Aswal, S. K. Nayak, C. Majumdar, S. Chattopadhyay, S. K. Gupta and J. V. Yakhmi, *Chem. Phys. Lett.*, 2010, **485**, 137-141.
- 34 S. Z. Rahaman, S. Maikap, T.-C. Tien, H.-Y. Lee, W.-S. Chen, F. T. Chen, M.-J. Kao and M.-J. Tsai, *Nanoscale Res. Lett.*, 2012, **7**, 345, 311 pp.
- 10 35 (a) W. Sinha, N. Deibel, A. Garai, D. Schweinfurth, S. Anwar, C. S. Purohit, B. Sarkar and S. Kar, *Dyes and Pigments*, 2014, **107**, 29-37; (b) W. Sinha, M. Kumar, A. Garai, C. S. Purohit, T. Som and S. Kar, *Dalton Trans.*, 2014, **43**, 12564-12573; (c) W. Sinha, N. Deibel, H. Agarwala, A. Garai, D. Schweinfurth, C. S. Purohit, G. K. Lahiri, B. Sarkar and S. Kar, *Inorg. Chem.*, 2014, **53**, 1417-1429; (d) W. Sinha, M.G. Sommer, N. Deibel, F. Ehret, B. Sarkar and S. Kar, *Chem. Eur. J.*, 2014, in press.
- 15 36 (a) D. V. Konarev, A. Y. Kovalevsky, X. Li, I. S. Neretin, A. L. Litvinov, N. y. V. Drichko, Y. L. Slovokhotov, P. Coppens and R. N. Lyubovskaya, *Inorg. Chem.*, 2002, **41**, 3638-3646; (b) H. Imahori, N. V. Tkachenko, V. Vehmanen, K. Tamaki, H. Lemmetyinen, Y. Sakata and S. Fukuzumi, *J. Phys. Chem. A*, 2001, **105**, 1750-1756.
- 20 37 N. V. Tkachenko, C. Guenther, H. Imahori, K. Tamaki, Y. Sakata, S. Fukuzumi and H. Lemmetyinen, *Chem. Phys. Lett.*, 2000, **326**, 344-350.
- 38 A. Kretschmann, M.-M. Walz, K. Flechtner, H.-P. Steinrueck and J. M. Gottfried, *Chem. Commun. (Cambridge, U. K.)*, 2007, 568-570.
- 30 39 L. Wang, B. Liu, D. Liu, M. Yao, Y. Hou, S. Yu, T. Cui, D. Li, G. Zou, A. Iwasiewicz and B. Sundqvist, *Adv. Mater. (Weinheim, Ger.)*, 2006, **18**, 1883-1888.
- 40 S. M. Sze and K. K. Ng, *Physics of Semiconductor Devices*, Wiley, 2006.
- 35 41 M. Kumar, A. Kanjilal and T. Som, *AIP Adv.*, 2013, **3**, 092126/092121-092126/092129.
- 42 A. A. M. Farag, E. A. A. El-Shazly, M. Abdel Rafea and A. Ibrahim, *Sol. Energy Mater. Sol. Cells*, 2009, **93**, 1853-1859.
- 43 M. Gedikpinar, M. Cavas, Z. A. Alahmed and F. Yakuphanoglu, *Superlattices Microstruct.*, 2013, **59**, 123-132.
- 40 44 S. Patil, S. Datar, N. Rekha, S. K. Asha and C. V. Dharmadhikari, *Nanoscale*, 2013, **5**, 4404-4411.
- 45 Z. I. Zhilina, S. V. Vodzinskii and S. A. Andronati, *Ukr. Khim. Zh. (Russ. Ed.)*, 1990, **56**, 1084-1088.
- 45 46 G. M. Sheldrick, *Acta Crystallogr., Sect. A: Found. Crystallogr.*, 2008, **64**, 112-122.
- 47 d. S. P. Van and A. L. Spek, *Acta Crystallogr., Sect. A: Found. Crystallogr.*, 1990, **A46**, 194-201.
- 50